electronic reprint

STRUCTURAL BIOLOGY
COMMUNICATIONS

ISSN: 2053-230X
journals.iucr.org/f

Structure, activity and thermostability investigations of OXA-163, OXA-181 and OXA-245 using biochemical analysis, crystal structures and differential scanning calorimetry analysis

Bjarte Aarmo Lund, Ane Molden Thomassen, Trine Josefine Olsen Carlsen and Hanna-Kirsti S. Leiros

Acta Cryst. (2017). F**73**, 579–587

STRUCTURAL BIOLOGY COMMUNICATIONS

ISSN 2053-230X

Structure, activity and thermostability investigations of OXA-163, OXA-181 and OXA-245 using biochemical analysis, crystal structures and differential scanning calorimetry analysis

Bjarte Aarmo Lund, Ane Molden Thomassen, Trine Josefine Olsen Carlsen and Hanna-Kirsti S. Leiros*

Department of Chemistry, UiT The Arctic University of Norway, 9037 Tromsø, Norway. *Correspondence e-mail: hanna-kirsti.leiros@uit.no

Received 21 July 2017
Accepted 25 September 2017

Edited by P. Dunten, Stanford Synchrotron Radiation Lightsource, USA

Keywords: antibiotic resistance; thermostability; enzyme kinetics; X-ray crystal structure; carbapenemase; β-lactamase; OXA-181; OXA-163; OXA-245.

PDB references: OXA-163, 5odz; OXA-181, 5oe0; OXA-245, 5oe2

Supporting information: this article has supporting information at journals.iucr.org/f

The first crystal structures of the class D β-lactamases OXA-181 and OXA-245 were determined to 2.05 and 2.20 Å resolution, respectively; in addition, the structure of a new crystal form of OXA-163 was resolved to 2.07 Å resolution. All of these enzymes are OXA-48-like and have been isolated from different clinical *Klebsiella pneumoniae* strains and also from other human pathogens such as *Pseudomonas aeruginosa* and *Escherichia coli*. Here, enzyme kinetics and thermostability studies are presented, and the new crystal structures are used to explain the observed variations. OXA-245 had the highest melting point (T_m = 55.8°C), as determined by differential scanning calorimetry, compared with OXA-163 (T_m = 49.4°C) and OXA-181 (T_m = 52.6°C). The differences could be explained by the loss of two salt bridges in OXA-163, and an overall decrease in the polarity of the surface of OXA-181 compared with OXA-245.

1. Introduction

After 70 years, penicillin and other β-lactam antibiotics are still the best weapons for fighting bacterial infections; however, the rise of bacterial strains resistant to β-lactam antibiotics threatens to make them obsolete (O'Neill, 2016; Bush & Macielag, 2010). The most common mechanisms for bacteria to become resistant to β-lactam antibiotics is the uptake of foreign genetic material encoding β-lactamases: enzymes that break down the central β-lactam ring of these antibiotics, rendering them inactive (Bush & Bradford, 2016).

To date (June 2017), over 2600 β-lactamases have been described (Bush, 2013*a*; http://bldb.eu). Based on their genetic sequence and structural motifs, β-lactamases can be grouped into four classes: A–D (Hall & Barlow, 2005; Bush, 2013*b*). The largest class, with more than 500 members, is class D. This class is often referred to as the oxacillinases (OXAs) owing to their preferential hydrolysis of oxacillin. Typically, this class has not been considered to be as threatening as the other classes. Still, it contains members which may inactivate the entire spectrum of β-lactam antibiotics (Leonard *et al.*, 2013; Evans & Amyes, 2014; Docquier & Mangani, 2016).

One of the most geographically widespread members of the class D β-lactamases is OXA-48 (Vallejo *et al.*, 2016). OXA-48 and the increasing number of OXA-48-like variants have been called the 'phantom menace' owing to their broad substrate specificity and the difficulties in identifying bacteria expressing OXA-48-like enzymes (Poirel *et al.*, 2012). The OXA-48-like

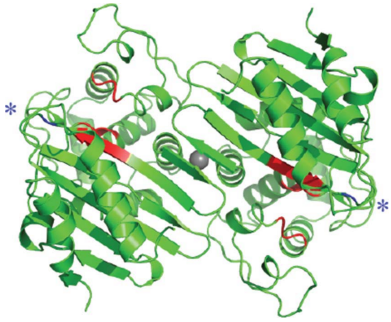

Table 1
Crystallization conditions for tOXA-163, tOXA-181 and tOXA-245.

	tOXA-163	tOXA-181	tOXA-245
Method	Vapour diffusion		
Plate type	Hampton Research VDX 24-well plate with sealant		
Temperature (K)	298		
Protein concentration (mg ml^{-1})	9	11	3
Buffer composition of protein solution	50 m*M* HEPES pH 7.2, 50 m*M* K_2SO_4	50 m*M* Tris pH 7.2, 50 m*M* K_2SO_4	25 m*M* HEPES pH 7.5
Composition of reservoir solution	0.1 *M* Tris pH 9.0, 28% PEG 500	0.1 *M* Tris pH 7.0, 0.2 *M* ammonium sulfate, 20.5% PEG MME 5000	0.1 *M* HEPES pH 7.0, 10% PEG 6000
Drop volume (µl)	2	1	2
Protein:reservoir ratio	3:20	1:1	1:1
Reservoir volume (µl)	1000	800	500

β-lactamases OXA-163, OXA-181 and OXA-245 have all been identified in *Klebsiella pneumoniae* (Potron, Nordmann *et al.*, 2011; Oteo *et al.*, 2013). Although *K. pneumoniae* is most commonly found in soil and water, it frequently causes infections in immunocompromised individuals and has been connected to outbreaks of nosocomial infections (Podschun & Ullmann, 1998; Paczosa & Mecsas, 2016; Navon-Venezia *et al.*, 2017). OXA-163 and OXA-181 have also been identified in other human pathogens such as *Escherichia coli* (McGann *et al.*, 2015; Stoesser *et al.*, 2016), and OXA-181 has been identified in *Pseudomonas aeruginosa* strains (Meunier *et al.*, 2016). OXA-181 is reported to originate from a *Shewanella xiamenensis* chromosomal β-lactamase (Potron, Poirel *et al.*, 2011) and OXA-163 also appears to originate from *Shewanella.* spp, while OXA-245 appears from random mutations of the OXA-48 gene in *K. pneumoniae* strains (Pérez-Vázquez *et al.*, 2016). OXA-163 was first identified in Argentina (Poirel *et al.*, 2011), but has also been observed in Egypt (Abdelaziz *et al.*, 2012). OXA-181 has been identified all over the world (Potron, Nordmann *et al.*, 2011; Samuelsen *et al.*, 2013; Rojas *et al.*, 2017). The strain responsible for OXA-245, however, appears to be limited to Spain (Pérez-Vázquez *et al.*, 2016). The sequence identities compared with OXA-48 are 98.0% for OXA-163, 98.4% for OXA-181 and 99.6% for OXA-245, using Gly22 (left after TEV cleavage) and the periplasmic part (Lys23–Pro256) for all four enzymes.

While class D β-lactamases are a diverse class with respect to protein sequence, their tertiary structures are highly conserved. All known structures of OXAs share an $\alpha\beta$-fold and many form dimers in solution (Docquier *et al.*, 2009; Paetzel *et al.*, 2000; Dale & Smith, 1976). The active site of OXAs is made up of three conserved motifs, $_{70}$STFK$_{73}$, $_{118}$SVV$_{120}$ and $_{208}$KTG$_{210}$, and each monomer has an independent active site. The serine in the STFK motif has been identified as the nucleophile that is responsible for the formation of the acyl-complex with β-lactam antibiotics (Paetzel *et al.*, 2000), while the lysine in the same motif has a conserved post-translational carboxylation that is important for deacetylation (Schneider *et al.*, 2009). The structures of the homologues OXA-48, OXA-163, OXA-232 and OXA-405 have been published (Docquier *et al.*, 2009; Stojanoski *et al.*, 2015). In this study, we wanted to thoroughly characterize the antibiotic-resistance enzymes OXA-163, OXA-181 and OXA-245 by comparing their thermostabilities, hydrolytic properties and crystal structures with those of the OXA-48 enzyme with worldwide spread.

2. Materials and methods

2.1. Cloning of OXA-181 and OXA-245 and recombinant macromolecule production

Genes encoding OXA-181 and OXA-245 were amplified from clinical isolates and cloned into a pDEST-17 vector using exponential megaprimer cloning (EMP) as described previously (Lund *et al.*, 2014, 2016). Two gene constructs were made for both OXA-181 and OXA-245, in which one gene construct encoded the full-length gene with the signal peptide, thus including residues 1–265 (nOXA-181 and nOXA-245), and a second gene construct encoded a truncated gene with a hexahistidine (His) tag and a TEV protease site followed by residues 23–265 (tOXA-181 and tOXA-245).

Synthetic DNA encoding an OXA-163 construct with a TEV protease site (ENLYFQG) followed by residues Lys23–Pro265 (tOXA-163), codon-optimized for expression in *E. coli*, was purchased from Life Technologies (Thermo Fisher Scientific). The DNA was inserted in pDEST17, which carries an N-terminal His tag. The primers and strains used in this study are described in Supplementary Table S1.

All enzymes were produced recombinantly. tOXA-181 and tOXA-163 were produced in *E. coli* BL21 (DE3) pLysS cells in Terrific Broth medium (TB) with 100 µg ml^{-1} ampicillin and 34 µg ml^{-1} chloramphenicol, the cells were induced by 0.4 m*M* isopropyl β-D-1-thiogalactopyranoside (VWR) at log phase and expression was continued at 20°C for 16 h. nOXA-181, nOXA-245 and tOXA-245 were produced in *E. coli* BL21 Star (DE3) pRARE cells in ZYP5052 autoinduction medium at 310 K (37°C) for 3–4 h and then left at 293 K (20°C) for 16 h.

Recombinant nOXA-181 and nOXA-245 were isolated from the periplasm after lysozyme treatment and were purified by two steps using an anion exchanger (Giuliani *et al.*, 2005). Contaminants were bound on an anion-exchange Q Sepharose column at 277 K (4°C) equilibrated with 25 m*M* bis-tris propane pH 7.2. The pH of the running buffer was adjusted to pH 9.5 before applying a pH gradient from pH 9.5 to 6.5 with 25 m*M* bis-tris propane. A cation-exchange column (HiTrap SP) was used for polishing with a gradient from pH 6.5 (25 m*M* HEPES) to pH 8.5 (25 m*M* HEPES) with 150 m*M*

Table 2
X-ray data-collection and processing statistics for tOXA-163, tOXA-181 and tOXA-245.

Values in parentheses are for the outer resolution shell.

	tOXA-163	tOXA-181	tOXA-245
Diffraction source	BL14.1, BESSY	BL14.1, BESSY	BL14.1, BESSY
Wavelength (Å)	0.918409	0.918409	0.918409
Temperature (K)	100	100	100
Detector	PILATUS 6M	PILATUS 6M	PILATUS 6M
Crystal-to-detector distance (mm)	293.51	426.55	371.19
Rotation range per image (°)	0.1	0.1	0.1
Total rotation range (°)	200	120	200
Exposure time per image (s)	0.4	0.3	0.3
Space group	$P6_522$	$P6_2$	$P2_1$
a, b, c (Å)	121.92, 121.92, 160.43	143.93, 143.93, 53.543	64.16, 108.72, 83.68
α, β, γ (°)	90, 90, 120	90, 90, 120	90, 102.39, 90
Mosaicity (°)	0.12	0.08	0.13
Resolution range (Å)	24.49–2.07 (2.14–2.07)	35.98–2.05 (2.12–2.05)	41.06–2.20 (2.28–2.20)
Total No. of reflections	476104 (48568)	258749 (26225)	211084 (21915)
No. of unique reflections	43401 (4244)	40027 (3911)	56510 (5674)
Completeness (%)	99.90 (100.00)	99.55 (99.21)	99.25 (99.95)
Multiplicity	11.0 (11.4)	6.5 (6.6)	3.7 (3.9)
$\langle I/\sigma(I)\rangle$	12.66 (2.98)	13.19 (2.27)	11.15 (3.63)
R_{meas}	0.1614 (0.8966)	0.08461 (0.8693)	0.0954 (0.387)
Overall B factor from Wilson plot (Å^2)	24.49	29.65	29.30

potassium sulfate. Recombinant tOXA-163, tOXA-181 and tOXA-245 were isolated from sonicated and clarified samples, and were first purified by nickel immobilized metal-affinity chromatography (Ni-IMAC) at 277 K (4°C) with a 0–500 m*M* imidazole gradient also including 25 m*M* HEPES pH 6.5 and 50 m*M* potassium sulfate (Lund *et al.*, 2016). The semi-pure enzyme extract was then cleaved using in-house-purified TEV protease (with L56V, S135G, S219N, T17S, N68D and I77V mutations; Leiros *et al.*, 2014) to remove the His tag, and the cleaved protein was again purified using Ni-IMAC, with the cleaved protein eluting in the flowthrough (Lund *et al.*, 2016; Leiros *et al.*, 2014). The last polishing step was a cation-exchange column as described for the enzyme isolated from the periplasm. Finally, the TEV constructs were dialysed in different storage buffers (Table 1), and nOXA-181 and nOXA245 were dialysed in 50 m*M* HEPES pH 7.2, 50 m*M* potassium sulfate. The proteins were concentrated using Centriprep centrifugal filters (Merck) and the protein concentrations were measured using the OD_{280}, molecular weights (MW) and extinction coefficients for each gene construct.

2.2. Enzyme kinetics of nOXA-181 and nOXA-245

Enzyme characterization and determination of the kinetic parameters were carried out as previously described for nOXA-48 (Antunes *et al.*, 2014; Lund *et al.*, 2016). Substrate hydrolysis was measured by monitoring the UV absorbance for ampicillin ($\Delta\varepsilon_{235\,nm} = -820\ M^{-1}\,cm^{-1}$, 1–100 µ*M*, 100 p*M* nOXA-181/nOXA-245); ceftazidime ($\Delta\varepsilon_{260\,nm} = -9000\ M^{-1}\,cm^{-1}$, 18–300 µ*M*, 5 n*M* nOXA-181/10 n*M* nOXA-245); ertapenem ($\Delta\varepsilon_{300\,nm} = -6920\ M^{-1}\,cm^{-1}$, 10–1000 µ*M*, 5 n*M* nOXA-181/nOXA-245); imipenem ($\Delta\varepsilon_{300\,nm} = -9000\ M^{-1}\,cm^{-1}$, 1–100 µ*M*, 5 n*M* nOXA-181/nOXA-245) and meropenem ($\Delta\varepsilon_{300\,nm} = -6500\ M^{-1}\,cm^{-1}$, 0.02–50 µ*M*, 5 n*M* nOXA-181/2 n*M* OXA-245). A SpectraMax M2e (Molecular Devices, Sunnyvale, California, USA) plate reader at 25°C and nonlinear regression using *GraphPad Prism* 6 (GraphPad Software) were used to determine k_{cat} and K_m with substrate-hydrolysis velocities from the linear phase of the reaction course.

2.3. Thermostability analysis by differential scanning calorimetry (DSC)

Purified tOXA-48 (Lund *et al.*, 2016), tOXA-163, tOXA-181 and tOXA-245 were dialyzed against 50 m*M* HEPES pH 7.0 supplemented with 50 m*M* potassium sulfate. Enzyme concentrations were in the range 0.5–1 mg ml^{-1}. All samples were filtrated and degassed. Temperatures were scanned in the range 10–80°C with a gradient of 1°C min^{-1}. To calculate the heat capacities the concentrations and molecular weights were given for the dimers. All measurements were collected using a CSC Nano-Differential Scanning Calorimeter III (N-DSC III) with the pressure kept constant at 304 kPa. All data were analyzed in *NanoAnalyze* 3.6 (TA Instruments, New Castle, Delaware, USA).

2.4. Crystallization conditions

tOXA-163, tOXA-181 and tOXA-245 were used for crystallization experiments. Conditions for tOXA-163 (9 mg ml^{-1}) and tOXA-181 (11 mg ml^{-1}) were identified from screening 284 in-house stochastic crystallization conditions, whereas the conditions for tOXA-245 (3 mg ml^{-1}) were based on the conditions for the tOXA-48 homologue. Ethanediol was added to the crystallization condition at 17, 20 and 25% to cryoprotect tOXA-163, tOXA-181 and tOXA-245, respectively, prior to flash-cooling the crystals in liquid nitrogen. Crystallization information is summarized in Table 1.

Table 3
Refinement statistics for tOXA-163, tOXA-181 and tOXA-245.

Values in parentheses are for the outer shell.

	tOXA-163	tOXA-181	tOXA-245
Resolution range (Å)	24.49–2.07 (2.14–2.07)	35.98–2.05 (2.12–2.05)	41.06–2.20 (2.28–2.20)
Completeness (%)	99.90 (100.00)	99.55 (99.21)	99.25 (99.95)
No. of reflections			
Working set	43401 (4244)	39856 (3913)	56501 (5674)
Test set	2186 (222)	1971 (165)	1290 (129)
Final R_{cryst}	0.1456 (0.1821)	0.2034 (0.3398)	0.1951 (0.2304)
Final R_{free}	0.1870 (0.2014)	0.2418 (0.4248)	0.2307 (0.2924)
No. of non-H atoms			
Protein	3975	3956	7944
Ligands	17	6	3
Water	367	476	536
Total	4359	4438	8483
R.m.s. deviations			
Bonds (Å)	0.014	0.003	0.004
Angles (°)	1.38	0.54	0.86
Average B factors (Å^2)			
Overall	32.84	37.78	39.04
Protein	31.88	36.68	38.87
Ligands	54.98	76.17	25.01
Water	42.28	46.40	41.65
Ramachandran plot			
Most favoured (%)	97.22	97.89	97.5
Allowed (%)	2.78	2.11	2.5

2.5. X-ray data collection and processing

X-ray diffraction data were collected on BL14.1 operated by the Helmholtz-Zentrum Berlin (HZB) at the BESSY II electron-storage ring (Berlin-Adlershof, Germany; Mueller *et al.*, 2015). Images were indexed and integrated using *XDS* (Kabsch, 2010) and were merged and scaled using *AIMLESS* (Evans & Murshudov, 2013). 5% of reflections were used for cross-validation for tOXA-163 and tOXA-181, whereas 2% were used for tOXA-245. X-ray data-collection and processing statistics are summarized in Table 2.

2.6. Structure solution and refinement

The structures were solved using *Phaser* (McCoy *et al.*, 2007) with one monomer of OXA-48 (PDB entry 3hbr; Docquier *et al.*, 2009) as the search model. Refinement was carried out using *phenix.refine* (Afonine *et al.*, 2012), with individual isotropic B factors and torsion-angle NCS restraints. Models were inspected and manually modified using *Coot* (Emsley *et al.*, 2010). For the final refinement, TLS parameters were refined and refinement weights were optimized. Refinement statistics are summarized in Table 3. Interactions within each protein were evaluated using the *Protein Interactions Calculator* (*PIC*; Tina *et al.*, 2007) and the *Protein Interfaces, Surfaces and Assemblies* service *PISA* at the European Bioinformatics Institute (http://www.ebi.ac.uk/pdbe/prot_int/pistart.html; Krissinel & Henrick, 2007). Figures were prepared using *PyMOL* (v1.8; Schrödinger).

3. Results and discussion

3.1. Enzyme production and enzyme kinetics

In this paper two gene constructs were used: either with native leader sequences followed by periplasmic purification (nOXA-181 and nOXA-245) or His-TEV gene constructs (tOXA-163, tOXA-181 and tOXA.245), where the His tag was cleaved with TEV protease. All gene constructs were expressed in *E. coli.* The highest yield was obtained for tOXA-181, with up to 55 mg of enzyme per litre in BL21 (DE3) pLysS cells in TB medium. tOXA-163 was expressed in BL21 (DE3) pLysS cells in TB medium, whereas nOXA-181,

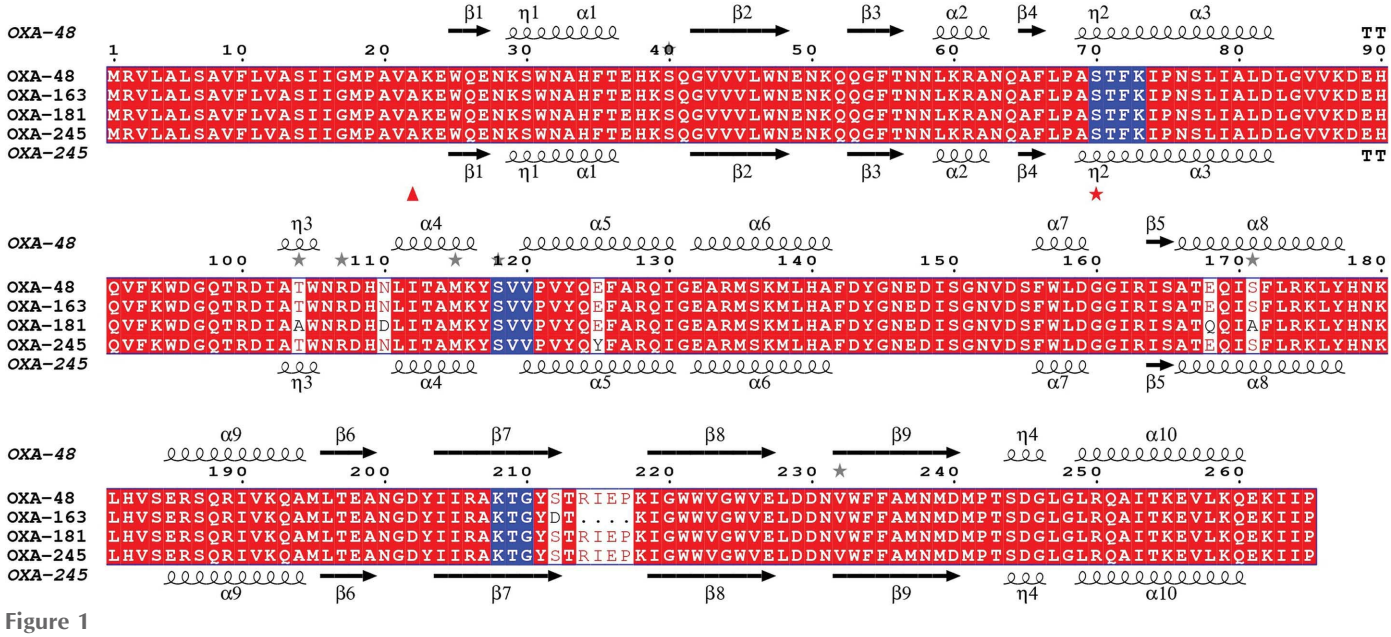

Figure 1
Sequence alignment of OXA-48, OXA-163, OXA-181 and OXA-245. The conserved active-site motifs are marked in blue. Secondary-structure elements are from the crystal structures of tOXA-48 (top; PDB entry 5dtk) and tOXA-245 (bottom; PDB entry 5oe2). The red triangle denotes the end of the signal peptide. The red star denotes the active-site serine. Grey stars indicate residues with alternate conformations in the crystal structure of OXA-48. This figure was prepared using *ESPript* 3.0 (Robert & Gouet, 2014).

Table 4
Kinetic parameters of purified nOXA-181 and nOXA-245 with standard errors from three replicates, showing similar hydrolytic properties compared with nOXA-48.

Results for nOXA-48 and OXA-163 are included for reference (Lund *et al.*, 2016; Poirel *et al.*, 2011).

	Penicillin	Cephalosporin	Carbapenems		
	Ampicillin	Ceftazidime	Ertapenem	Imipenem	Meropenem
nOXA-181					
K_m (μ*M*)	23 ± 5	170 ± 90	900 ± 300	17 ± 4	0.3 ± 0.1
k_{cat} (s^{-1})	2100 ± 200	0.7 ± 0.2	1.6 ± 0.3	5.1 ± 0.4	0.013 ± 0.01
k_{cat}/K_m (μM^{-1} s^{-1})	91	0.004	0.002	0.3	0.04
nOXA-245					
K_m (μ*M*)	35 ± 13	110 ± 80	80 ± 20	11 ± 1	2 ± 0.8
k_{cat} (s^{-1})	1200 ± 200	0.3 ± 0.1	0.29 ± 0.03	4.4 ± 0.2	0.11 ± 0.01
k_{cat}/K_m (μM^{-1} s^{-1})	34	0.003	0.004	0.40	0.05
nOXA-48†					
K_m (μ*M*)	150	5100	100	7.9	1
k_{cat} (s^{-1})	560	4	0.13	4.5	0.1
k_{cat}/K_m (μM^{-1} s^{-1})	4	0.0008	0.001	0.6	0.1
OXA-163‡					
K_m (μ*M*)	320	>2000	150	530	2200
k_{cat} (s^{-1})	25	200	0.01	0.03	0.07
k_{cat}/K_m (μM^{-1} s^{-1})	0.1	<0.1	0.00007	0.00006	0.00003

† The enzyme kinetic parameters for nOXA-48 with ampicillin, imipenem and meropenem are from Lund *et al.* (2016), those with ceftazidime are from Poirel *et al.* (2004) and those with ertapenem are from Docquier *et al.* (2009). ‡ The enzyme kinetic parameters for OXA-163 are from Poirel *et al.* (2011).

nOXA-245 and tOXA-245 were expressed in BL21 STAR (DE3) pRARE cells in ZYP5052 autoinduction medium.

The substitutions in the protein sequence for OXA-181 and OXA-245 (Fig. 1) are located away from the active-site residues (Fig. 3), and none of the conserved motifs $_{70}$STFK$_{73}$, $_{118}$SVV$_{120}$ or $_{208}$KTG$_{210}$ appear to be influenced. However, it is well known that modifications of distal sites may influence enzyme activity (Guarnera & Berezovsky, 2016), so we enzymatically characterized nOXA-181 and nOXA-245 and compared our results with the reported values for OXA-48 (Lund *et al.*, 2016; Docquier *et al.*, 2009; Poirel *et al.*, 2004) and OXA-163 (Poirel *et al.*, 2011). We tested the substrates ampicillin, ceftazidime, ertapenem, imipenem and meropenem. Both enzymes showed activity against all of the substrates (Table 4); however, ceftazidime was a poor substrate. In summary, the substitutions in nOXA-181 and nOXA-245 did not significantly change the enzymatic characteristics compared with OXA-48. OXA-163, however, has an overall lower catalytic efficiency, but much higher turnover rates for ceftazidime.

3.2. Thermostability analysis by differential scanning calorimetry

Even though the enzyme kinetics did not reveal any significant functional changes between nOXA-181 and nOXA-245, an investigation of thermostability properties could still reveal differences. We determined the midpoint melting temperatures (T_m) for tOXA-48, tOXA-163, tOXA-181 and tOXA-245 by differential scanning calorimetry (DSC). Since all four enzymes are dimers according to interaction analysis of the crystal structures, with 10–20% of the surface buried up on dimerization (Krissinel & Henrick, 2007), and gel-filtration experiments of OXA-48 indicate dimer formation (data not shown), the curves were fitted with the molecular weights and concentrations of the dimers. The recorded melting curves (Fig. 2) and their fit to the two-state model (Supplementary Fig. S1) indicate that all four enzymes unfold *via* a two-state transition without a stable intermediate, like many other dimeric proteins (Neet & Timm, 1994). tOXA-163 and tOXA-181 have a broader melting curves than tOXA-48 and tOXA-245 (Fig. 2) possibly owing to lower protein concentrations, nonhomogeneous samples or minor impurities. Still, we found tOXA-163 to be the least stable of the OXA-48-like enzymes, with a T_m of 49.40°C compared with the other OXA-48-like enzymes with midpoint melting temperatures of 55.3°C (tOXA-48), 52.6°C (tOXA-181) and 55.8°C (tOXA-245) (Table 5, Fig. 2).

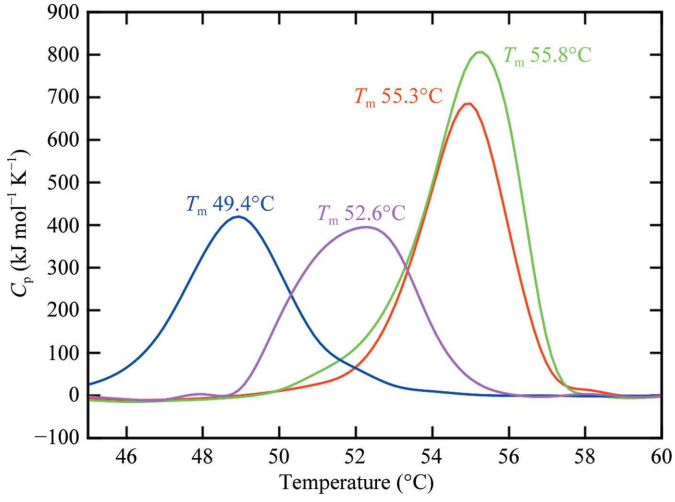

Figure 2
Differential scanning calorimetry curves for tOXA-48 (red), tOXA-163 (blue), tOXA-181 (purple) and tOXA-245 (green) showing that tOXA-245 and tOXA-48 have the highest melting temperatures, whereas tOXA-181 and tOXA-163 have lower melting points.

Table 5
Midpoint melting temperatures (T_m) determined by differential scanning calorimetry for tOXA-48, tOXA-163, tOXA-181 and tOXA-245.

T_m values are given as the mean with standard deviations from duplicate experiments performed in 50 m*M* HEPES pH 7.0 with 50 m*M* potassium sulfate. The apparent unfolding enthalpies (ΔH) with standard deviations were calculated for a two-state model with the enzymes modelled as dimers.

	T_m (°C)	ΔH (kJ mol^{-1})
tOXA-48	55.3 ± 0.2	1500 ± 200
tOXA-163	49.4 ± 0.1	1280 ± 50
tOXA-181	52.6 ± 0.1	1400 ± 300
tOXA-245	55.8 ± 0.1	1700 ± 100

3.3. New crystal structures of tOXA-181 and tOXA-245, and a new tOXA-163 crystal form resolved by X-ray crystallography

We present the first crystal structures of the OXA-48-like β-lactamases tOXA-181 and tOXA-245 and a new crystal form of tOXA-163. The new crystal form of tOXA-163 belonged to space group $P6_522$ and diffracted to 2.07 Å resolution, with R_{cryst} and R_{free} values of 0.15 and 0.19, respectively. The tOXA-181 enzyme crystallized in space group $P6_2$ and diffracted to 2.05 Å resolution, with R_{cryst} and R_{free} values of 0.20 and 0.24, respectively. Finally, tOXA-245 crystallized in space group $P2_1$ and diffracted to 2.20 Å resolution, with refined R_{cryst} and R_{free} values of 0.20 and 0.23, respectively. Gly22 from the TEV site is absent in all structures and Lys23 is missing in all tOXA-181 and tOXA-245 chains, but otherwise all residues are included in the final PDB models. The asymmetric unit of the new crystal structures are different (Fig. 3): tOXA-163 and tOXA-181 have a dimer in the asymmetric unit, corresponding to the expected biological assembly, while tOXA-245 has two dimers in the asymmetric unit. An interesting feature is the chloride ions that are observed to bridge two arginines at the dimer interface: one arginine from each monomer in all three new OXA structures. Other class D β-lactamases such as OXA-10 are known to have a cation-mediated dimerization with a histidine acid in the same position binding to a divalent cation such as cobalt, copper or zinc (Paetzel *et al.*, 2000; Danel *et al.*, 2001).

As expected from the sequence alignment (Fig. 1), the new structures show a close resemblance in their tertiary structure. The mutations are all on the surface of the proteins and the dimer interface is undisturbed. When all monomers of the new structures are compared against each other (tOXA-163, tOXA-181 and tOXA-245), the different chains in the asymmetric units have r.m.s.d. values for C^{α} atoms in the range 0.3–0.6 Å as calculated by the protein structure-similarity service *PDBeFold* at the European Bioinformatics Institute (Krissinel & Henrick, 2004).

3.4. The increased flexibility necessary for cephalosporin hydrolysis makes OXA-163 less stable

OXA-163 differs from OXA-48 by an S212D substitution and a four-amino-acid deletion corresponding to Arg214, Ile215, Glu216 and Pro217 in OXA-48. Crystal structures of OXA-163 have previously been reported (PDB entries 4s2l, 4s2m and 5har; Stojanoski *et al.*, 2015, 2016); however, we report a new space group and unit cell for our tOXA-163 structure, similar to a crystal form reported for a laboratory mutant of OXA-48 (PDB entry 5hap; Stojanoski *et al.*, 2016) crystallized from similar conditions. Comparing our tOXA-163 structure with another OXA-163 structure (PDB entry 4s2l) reveals perturbations that are localized primarily to polar surface residues, and there are two molecules in the asymmetric unit (Fig. 3). The r.m.s.d. for C^{α} atoms in one tOXA-163 chain compared with existing OXA-163 structures are: 0.32–0.43 Å for PDB entry 4s2l, 0.52–0.67 Å for PDB entry 4s2m and 0.32–0.46 Å for PDB entry 5har.

For tOXA-163, shortening the loop (Fig. 4) connecting β7 to β8 opens up access to the active site, allowing the binding of bulkier groups, as found in, for example, cephalosporins (Stojanoski *et al.*, 2015). From the enzymatic characterization (Table 4) it was clear that this structural change increases the catalytic turnover for the cephalosporin ceftazidime dramatically, but the carbapenemase enzyme activity is nearly abolished. The DSC results shows that tOXA-163 had a 5.9°C lower melting temperature compared with tOXA-48 (Table 5) and the structure shows that the deletion of residues 214–217 in tOXA-163 disrupts two ionic bonds, Arg214–Asp159

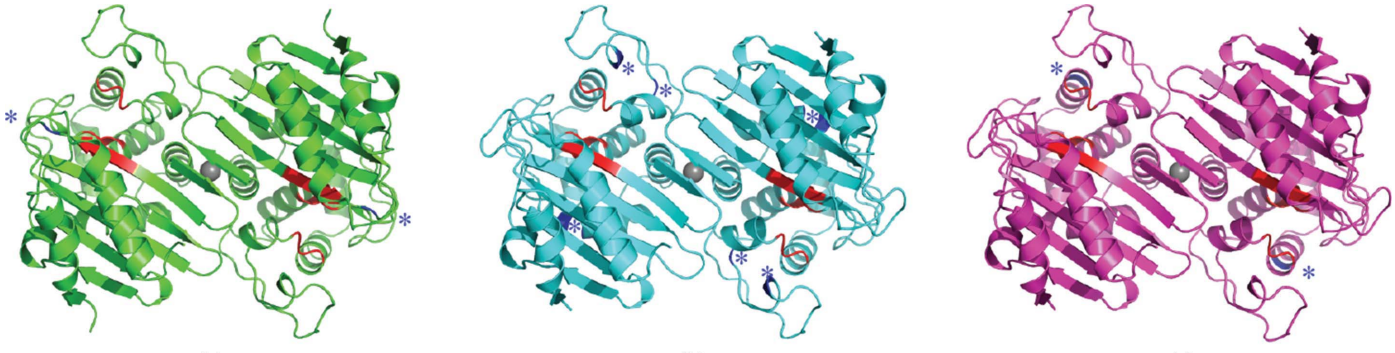

(*a*) (*b*) (*c*)

Figure 3
The quaternary structures of tOXA-163 (*a*), tOXA-181 (*b*) and tOXA-245 (*c*) reveal biological dimers with buried chloride ions in the dimer interface (grey). For OXA-245 there are two dimers in the asymmetric unit (one is shown). Active-site motifs are coloured in red and residues involved in substitutions are shown in blue and marked with asterisks.

(2.9 Å) and Glu216–Lys218 (2.4 Å), that are found in both tOXA-181 and tOXA-245 (Figs. 4*a*, 4*b* and 4*c*). The effect of the S212D mutation in OXA-163 seems to partially compensate for the loss of two ionic bonds by forming two hydrogen bonds from the Asp212 side chain to the main-chain N atoms of residue 218 and 219 rather than one as found in tOXA-181 and tOXA-245 (Figs. 4*a*, 4*b* and 4*c*). For OXA-163 it appears that the destabilization of the structure allows greater flexibility and easier access to the active site, facilitating the hydrolysis of bulky substrates (Simakov *et al.*, 2017).

3.5. OXA-181 reveals decreased thermostability

The OXA-181 enzyme differs from OXA-48 by four substitutions: T104A, N110D, E168Q and S171A. Our new structure was resolved to 2.05 Å resolution in space group $P6_2$, with two molecules in the asymmetric unit (Fig. 3). The tOXA-181 structure has very similar unit-cell parameters to some of the crystals of the homologues OXA-48 (PDB entry 4s2k; King *et al.*, 2015) and OXA-232 (PDB entry 5hfo; P. Retailleau, S. Oueslati, C. Cisse, P. Nordmann, T. Naas & B. Iorga, unpublished work), but the tOXA-181 crystals grew from different crystallization conditions.

The nOXA-181 enzyme has the highest activity against ampicillin of the tested OXAs and has some activity against ceftazidime (Table 4). The activity of nOXA-181 against the carbapenems is lower than that of nOXA-48; however, these *in vitro* results are not reflected in bacterial cells, where OXA-48 and OXA-181 have very similar hydrolytic profiles (Potron, Nordmann *et al.*, 2011).

For tOXA-181 the thermal stability was reduced by 2.7°C compared with tOXA-48 (Table 5) and this could be attributed to changes in the tertiary structure. The N110D mutation in tOXA-181 introduces an ionic bond from Asp110 to His90,

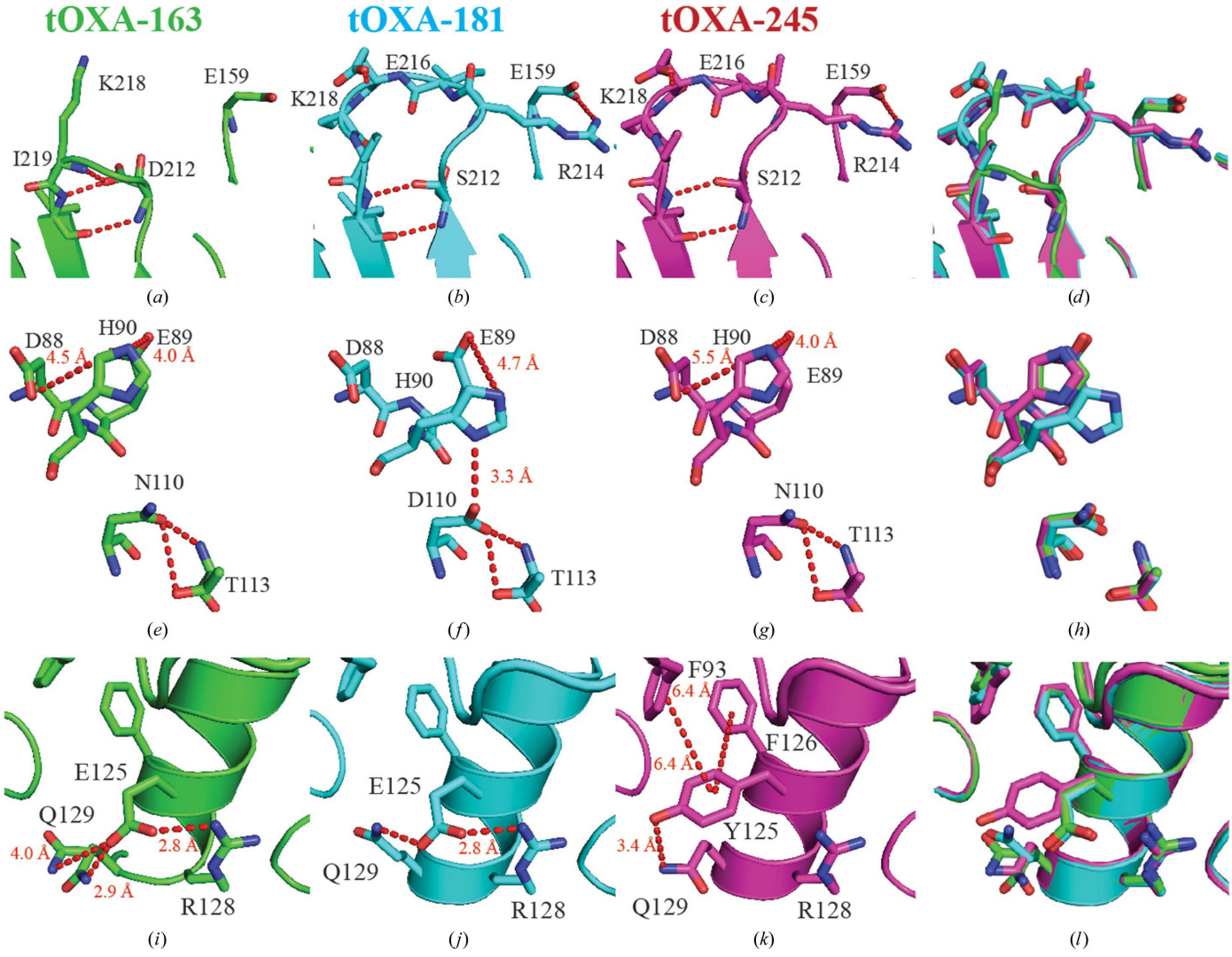

Figure 4
The substitutions in tOXA-163 (green), tOXA-181 (cyan) and tOXA-245 (magenta). (*a*), (*b*) and (*c*) show the S212D substitution and the deletion of residues 214–217 in tOXA-163 which disrupt two ionic bonds. (*e*), (*f*) and (*g*) show the N110D substitution in OXA-181; the aspartic acid forms an ionic bond to His90, which disrupts the Asp88-His90-Glu89 network. (*i*), (*j*) and (*k*) show the E125Y substitution in tOXA-245, where the loss of an ionic bond to Arg128 is compensated by π–π stacking from Tyr125 to both Phe93 and Phe126. (*d*), (*h*) and (*l*) show superpositions of tOXA-163 (green), tOXA-181 (cyan) and tOXA-245 (magenta) for comparison of the three structures.

causing the His90 residue to shift significantly. This disrupts the ionic network Asp88-His90-Glu89 as found in OXA-48 (not shown), tOXA-163 and tOXA-245 (Figs. 4*d*, 4*e* and 4*f*). The other OXA-181 mutations T104A and S171A decrease the overall polarity of the surface, which is likely to make the protein less stable (Vogt *et al.*, 1997; Michetti *et al.*, 2017), thus explaining the lower thermal stability of tOXA-181 compared with tOXA-48.

3.6. A new crystal structure of tOXA-245 uncovers a stabilizing aromatic network

OXA-245 differs from OXA-48 by the single substitution E125Y. The tOXA-245 crystal structure belonged to space group $P2_1$ with four molecules in the asymmetric unit and was refined to 2.20 Å resolution. tOXA-245 crystallized with similar unit-cell parameters to another crystal form of OXA-48 (PDB entry 3hbr).

In our substrate-hydrolysis experiments, nOXA-245 shows the same behaviour as nOXA-181, with higher activity against ampicillin compared with nOXA-48, some activity against ceftazidime and weaker carbapenemase activity than nOXA-48, except for the carbapenem ertapenem, towards which nOXA-245 had the highest activity of the tested OXAs (Table 4). This behaviour is consistent with the antibiotic-susceptibility profile reported previously (Oteo *et al.*, 2013).

tOXA-245 had an increased overall stability of 0.5°C compared with tOXA-48 (Table 5) and only has the E125Y substitution. This stabilization is surprising, since Glu125 in the other structures forms an ionic bond to Arg129 and a hydrogen bond to Gln129. However, in the tOXA-245 crystal structure Tyr125 makes a hydrogen bond to Gln129 with the phenolic hydroxyl group and π–π stacking interactions with Phe126 (6.0 Å between the ring centroids) and Phe93 (6.5 Å between the ring centroids). The π–π stacking from Phe93 to Phe126 and the hydrogen bond from the Gln129 amide N atom to the Tyr125 hydroxyl group may compensate for the loss of the ionic bond (Figs. 4*g*, 4*h* and 4*i*), and thus stabilize the protein and explain the observed 0.5°C increase in overall stability. π–π stacking has been reported in the literature to enhance the overall thermostability (Karlström *et al.*, 2006).

4. Conclusion

Overall, it appears that the changes in the nOXA-181 and nOXA-245 protein sequences are well tolerated, giving a similar hydrolytic spectrum compared with nOXA-48. In overall thermal stability, tOXA-163 was the least stable OXA-48-like enzyme, with a melting temperature reduced by 5.9°C compared with tOXA-48. Based on the crystal structures, we hypothesize that this decrease is caused by two broken salt bridges (Glu126–Arg128 and Glu159–Arg214) and a more accessible active site compared with the three other OXA enzymes. The tOXA-181 enzyme has a 2.7°C lower melting point compared with tOXA-48, possibly owing to one broken ionic interaction in the Asp88-His90-Glu89 network caused by the shift of His90 towards Asp110, combined with an overall decrease in surface polarity. Finally, tOXA-245 was most similar to tOXA-48, with an increased T_m of 0.5°C, and this increase could arise from one additional hydrogen bond (Tyr125–Asn129) and the π–π aromatic stacking network with Phe93-Tyr125-Phe126 compensating for the loss of the Glu125–Arg128 salt bridge.

From these observations, we speculate that a bacterium carrying a serine β-lactamase already has an advantage in β-lactam resistance, that the differences in the sequences of OXA-181 and OXA-245 depend on the original host organism, and that these differences are tolerated as long as there is no interference with substrate hydrolysis.

Acknowledgements

The provision of beam time at BL14.1, BESSY II, Berlin, Germany is highly valued. We thank Tony Christopeit and Ronny Helland for assistance with data collection. We thank Ørjan Samuelsen for the contribution of clinical isolates of OXA-181 and OXA-245. The authors declare no competing financial interests. Author contributions are as follows. BL and H-KSL designed the experiments; BAL, AMT and TJOC performed the cloning, expression and purification; BAL determined the kinetic parameters; BAL, AMT and H-KSL prepared and solved the crystal structures; AMT and BAL performed the DSC studies; BAL and H-KSL analysed the data and wrote the paper. All authors have given approval to the final version of the manuscript.

References

Abdelaziz, M. O., Bonura, C., Aleo, A., El-Domany, R. A., Fasciana, T. & Mammina, C. (2012). *J. Clin. Microbiol.* **50**, 2489–2491.
Afonine, P. V., Grosse-Kunstleve, R. W., Echols, N., Headd, J. J., Moriarty, N. W., Mustyakimov, M., Terwilliger, T. C., Urzhumtsev, A., Zwart, P. H. & Adams, P. D. (2012). *Acta Cryst.* D**68**, 352–367.
Antunes, N. T., Lamoureaux, T. L., Toth, M., Stewart, N. K., Frase, H. & Vakulenko, S. B. (2014). *Antimicrob. Agents Chemother.* **58**, 2119–2125.
Bush, K. (2013*a*). *Ann. N. Y. Acad. Sci.* **1277**, 84–90.
Bush, K. (2013*b*). *J. Infect. Chemother.* **19**, 549–559.
Bush, K. & Bradford, P. A. (2016). *Cold Spring Harb. Perspect. Med.* **6**, a025247.
Bush, K. & Macielag, M. J. (2010). *Expert Opin. Ther. Pat.* **20**, 1277–1293.
Dale, J. W. & Smith, J. T. (1976). *Biochem. Biophys. Res. Commun.* **68**, 1000–1005.
Danel, F., Paetzel, M., Strynadka, N. C. J. & Page, M. G. P. (2001). *Biochemistry*, **40**, 9412–9420.
Docquier, J.-D., Calderone, V., De Luca, F., Benvenuti, M., Giuliani, F., Bellucci, L., Tafi, A., Nordmann, P., Botta, M., Rossolini, G. M. & Mangani, S. (2009). *Chem. Biol.* **16**, 540–547.
Docquier, J.-D. & Mangani, S. (2016). *Curr. Drug Targets*, **17**, 1061–1071.
Emsley, P., Lohkamp, B., Scott, W. G. & Cowtan, K. (2010). *Acta Cryst.* D**66**, 486–501.
Evans, B. A. & Amyes, S. G. B. (2014). *Clin. Microbiol. Rev.* **27**, 241–263.
Evans, P. R. & Murshudov, G. N. (2013). *Acta Cryst.* D**69**, 1204–1214.
Giuliani, F., Docquier, J.-D., Riccio, M. L., Pagani, L. & Rossolini, G. M. (2005). *Antimicrob. Agents Chemother.* **49**, 1973–1980.
Guarnera, E. & Berezovsky, I. N. (2016). *Curr. Opin. Struct. Biol.* **37**, 1–8.

Hall, B. G. & Barlow, M. (2005). *J. Antimicrob. Chemother.* **55**, 1050–1051.
Kabsch, W. (2010). *Acta Cryst.* D**66**, 125–132.
Karlström, M., Steen, I. H., Madern, D., Fedöy, A. E., Birkeland, N. K. & Ladenstein, R. (2006). *FEBS J.* **273**, 2851–2868.
King, D. T., King, A. M., Lal, S. M., Wright, G. D. & Strynadka, N. C. J. (2015). *ACS Infect. Dis.* **1**, 175–184.
Krissinel, E. & Henrick, K. (2004). *Acta Cryst.* D**60**, 2256–2268.
Krissinel, E. & Henrick, K. (2007). *J. Mol. Biol.* **372**, 774–797.
Leiros, H. K. S., Skagseth, S., Edvardsen, K. S. W., Lorentzen, M. S., Bjerga, G. E. K., Leiros, I. & Samuelsen, Ø. (2014). *Antimicrob. Agents Chemother.* **58**, 4826–4836.
Leonard, D. A., Bonomo, R. A. & Powers, R. A. (2013). *Acc. Chem. Res.* **46**, 2407–2415.
Lund, B. A., Christopeit, T., Guttormsen, Y., Bayer, A. & Leiros, H.-K. S. (2016). *J. Med. Chem.* **59**, 5542–5554.
Lund, B. A., Leiros, H.-K. S. & Bjerga, G. E. (2014). *Microb. Cell Fact.* **13**, 38.
McCoy, A. J., Grosse-Kunstleve, R. W., Adams, P. D., Winn, M. D., Storoni, L. C. & Read, R. J. (2007). *J. Appl. Cryst.* **40**, 658–674.
McGann, P., Snesrud, E., Ong, A. C., Appalla, L., Koren, M., Kwak, Y. I., Waterman, P. E. & Lesho, E. P. (2015). *Antimicrob. Agents Chemother.* **59**, 3556–3562.
Meunier, D., Doumith, M., Findlay, J., Mustafa, N., Mallard, K., Anson, J., Panagea, S., Pike, R., Wright, L., Woodford, N. & Hopkins, K. L. (2016). *J. Antimicrob. Chemother.* **71**, 2056–2057.
Michetti, D., Brandsdal, B. O., Bon, D., Isaksen, G. V., Tiberti, M. & Papaleo, E. (2017). *PLoS One*, **12**, e0169586.
Mueller, U., Förster, R., Hellmig, M., Huschmann, F. U., Kastner, A., Malecki, P., Pühringer, S., Röwer, M., Sparta, K., Steffien, M., Ühlein, M., Wilk, P. & Weiss, M. S. (2015). *Eur. Phys. J. Plus*, **130**, 141.
Navon-Venezia, S., Kondratyeva, K. & Carattoli, A. (2017). *FEMS Microbiol. Rev.* **41**, 252–275.
Neet, K. E. & Timm, D. E. (1994). *Protein Sci.* **3**, 2167–2174.
O'Neill, J. (2016). *Tackling Drug-Resistant Infections Globally: Final Report and Recommendations.* London: Review on Antimicrobial Resistance. https://amr-review.org/sites/default/files/160525_Final paper_with cover.pdf.
Oteo, J. *et al.* (2013). *J. Antimicrob. Chemother.* **68**, 317–321.
Paczosa, M. K. & Mecsas, J. (2016). *Microbiol. Mol. Biol. Rev.* **80**, 629–661.
Paetzel, M., Danel, F., de Castro, L., Mosimann, S. C., Page, M. G. P. & Strynadka, N. C. J. (2000). *Nature Struct. Biol.* **7**, 918–925.
Pérez-Vázquez, M., Oteo, J., García-Cobos, S., Aracil, B., Harris, S. R., Ortega, A., Fontanals, D., Hernández, J. M., Solís, S., Campos, J., Dougan, G. & Kingsley, R. A. (2016). *J. Antimicrob. Chemother.* **71**, 887–896.
Podschun, R. & Ullmann, U. (1998). *Clin. Microbiol. Rev.* **11**, 589–603.
Poirel, L., Castanheira, M., Carrër, A., Rodriguez, C. P., Jones, R. N., Smayevsky, J. & Nordmann, P. (2011). *Antimicrob. Agents Chemother.* **55**, 2546–2551.
Poirel, L., Héritier, C., Tolün, V. & Nordmann, P. (2004). *Antimicrob. Agents Chemother.* **48**, 15–22.
Poirel, L., Potron, A. & Nordmann, P. (2012). *J. Antimicrob. Chemother.* **67**, 1597–1606.
Potron, A., Nordmann, P., Lafeuille, E., Al Maskari, Z., Al Rashdi, F. & Poirel, L. (2011). *Antimicrob. Agents Chemother.* **55**, 4896–4899.
Potron, A., Poirel, L. & Nordmann, P. (2011). *Antimicrob. Agents Chemother.* **55**, 4405–4407.
Robert, X. & Gouet, P. (2014). *Nucleic Acids Res.* **42**, W320–W324.
Rojas, L. J., Hujer, A. M., Rudin, S. D., Wright, M. S., Domitrovic, T. N., Marshall, S. H., Hujer, K. M., Richter, S. S., Cober, E., Perez, F., Adams, M. D., van Duin, D. & Bonomo, R. A. (2017). *Antimicrob. Agents Chemother.* **61**, e00454-17.
Samuelsen, Ø., Naseer, U., Karah, N., Lindemann, P. C., Kanestrom, A., Leegaard, T. M. & Sundsfjord, A. (2013). *J. Antimicrob. Chemother.* **68**, 1682–1685.
Schneider, K. D., Bethel, C. R., Distler, A. M., Hujer, A. M., Bonomo, R. A. & Leonard, D. A. (2009). *Biochemistry*, **48**, 6136–6145.
Simakov, N., Leonard, D. A., Smith, J. C., Wymore, T. & Szarecka, A. (2017). *J. Phys. Chem. B*, **121**, 3285–3296.
Stoesser, N., Sheppard, A. E., Peirano, G., Sebra, R., Lynch, T., Anson, L., Kasarskis, A., Motyl, M. R., Crook, D. W. & Pitout, J. D. (2016). *Antimicrob. Agents Chemother.* **60**, 6948–6951.
Stojanoski, V., Adamski, C. J., Hu, L., Mehta, S. C., Sankaran, B., Zwart, P., Prasad, B. V. V. & Palzkill, T. (2016). *Biochemistry*, **55**, 2479–2490.
Stojanoski, V., Chow, D.-C., Fryszczyn, B., Hu, L. Y., Nordmann, P., Poirel, L., Sankaran, B., Prasad, B. V. V. & Palzkill, T. (2015). *Biochemistry*, **54**, 3370–3380.
Tina, K. G., Bhadra, R. & Srinivasan, N. (2007). *Nucleic Acids Res.* **35**, W473–W476.
Vallejo, J. A., Martínez-Guitián, M., Vázquez-Ucha, J. C., González-Bello, C., Poza, M., Buynak, J. D., Bethel, C. R., Bonomo, R. A., Bou, G. & Beceiro, A. (2016). *J. Antimicrob. Chemother.* **71**, 2171–2180.
Vogt, G., Woell, S. & Argos, P. (1997). *J. Mol. Biol.* **269**, 631–643.

Supporting information

Table S1 Macromolecule production information for the cloning and production of OXA-163,OXA-181 and OXA-245. Italic nucleotides

Source organism	*Klebsiella pneumoniae*	
DNA source	Genomic DNA	
Forward primer	**Native construct with signal peptide:** **OXAs:** ATAATTTTGTTTAACTTTAAGA AGGAGATATACATATGCGTGT ATTAGCCTTATC GG	**His-tagged construct with TEV-protease cleavage site:** **TEV-cleavage site[a]:** ACCATCACCTCGAATCAACAAGTTTG TAC*GGTGAGAATCTTTATTTTC GGGT*T **OXAs:** GTTTGTACGGTGAGAATCTTTATTTT CAGGGTAAGGAATGGCAAGAAAACA AAAGT
Reverse primer	**OXAs:** GGCTTTGTTAGCAG CCTCGAATCACTAGGGAATAA TTTTTTCCTGTTTGAG	**TEV-cleavage site[a]:** GGCTTTGTTAGCAGCCTCGAATCA*AC CCTGAAAATAAAGATTCTCACCG* **OXAs:** GGCTTTGTTAGCAGCCTCGAATCACT AGGGAATAATTTTTTCCTGTTTGAG
EMP R2 primer	TTCTAGAGGGAAACCGTTGTG GTCT	TTGTTGATTCGAGGTGATGGTGAT
Cloning vector	pDEST17	
Expression vector	pDEST17	
Expression host	*E. coli* BL21 (DE3) STAR pRARE	
Complete amino acid sequence of the construct produced[a]		
OXA-163[b]		**(tOXA-163)** HHHHHHENLYFQGKEWQENKSWNAHF TEHKSQGVVVLWNENKQQGFTNNLKR ANQAFLPASTFKIPNSLIALDLGVVKDE HQVFKWDGQTRDIATWNRDHNLITAM KYSVVPVYQEFARQIGEARMSKMLHAF DYGNEDISGNVDSFWLDGGIRISATEQIS

		FLRKLYHNKLHVSERSQRIVKQAMLTE ANGDYIIRAKTGYDTKIGWWVGWVEL DDNVWFFAMNMDMPTSDGLGLRQAIT KEVLKQEKIIP
OXA-181	**(nOXA-181**) <u>MRVLALSAVFLVASIIGMPAVA</u> KEWQENKSWNAHFTEHKSQG VVVLWNENKQQGFTNNLKRA NQAFLPASTFKIPNSLIALDLGV VKDEHQVFKWDGQTRDIAAW NRDHDLITAMKYSVVPVYQEF ARQIGEARMSKMLHAFDYGNE DISGNVDSFWLDGGIRISATQQI AFLRKLYHNKLHVSERSQRIVK QAMLTEANGDYIIRAKTGYSTR IEPKIGWWVGWVELDDNVWFF AMNMDMPTSDGLGLRQAITKE VLKQEKIIP	**(tOXA-181)** <u>MSYYHHHHHHLESTSLYGENLYFQ</u> GKEWQENKSWNAHFTEHKSQGVV VLWNENKQQGFTNNLKRANQAFLP ASTFKIPNSLIALDLGVVKDEHQVF KWDGQTRDIAAWNRDHDLITAMK YSVVPVYQEFARQIGEARMSKMLH AFDYGNEDISGNVDSFWLDGGIRIS ATQQIAFLRKLYHNKLHVSERSQRI VKQAMLTEANGDYIIRAKTGYSTRI EPKIGWWVGWVELDDNVWFFAMN MDMPTSDGLGLRQAITKEVLKQEKI IP
OXA-245	**(nOXA-245)** <u>MRVLALSAVFLVASIIGMPAVA</u> KEWQENKSWNAHFTEHKSQG VVVLWNENKQQGFTNNLKRA NQAFLPASTFKIPNSLIALDLGV VKDEHQVFKWDGQTRDIATW NRDHNLITAMKYSVVPVYQYF ARQIGEARMSKMLHAFDYGNE DISGNVDSFWLDGGIRISATEQI SFLRKLYHNKLHVSERSQRIVK QAMLTEANGDYIIRAKTGYSTR IEPKIGWWVGWVELDDNVWFF AMNMDMPTSDGLGLRQAITKE VLKQEKIIP	**(tOXA-245)** <u>MSYYHHHHHHLESTSLYGENLYFQ</u> GKEWQENKSWNAHFTEHKSQGVV VLWNENKQQGFTNNLKRANQAFLP ASTFKIPNSLIALDLGVVKDEHQVF KWDGQTRDIATWNRDHNLITAMK YSVVPVYQYFARQIGEARMSKMLH AFDYGNEDISGNVDSFWLDGGIRIS ATEQISFLRKLYHNKLHVSERSQRIV KQAMLTEANGDYIIRAKTGYSTRIE PKIGWWVGWVELDDNVWFFAMN MDMPTSDGLGLRQAITKEVLKQEKI IP

[a] The nucleotides in the TEV protease cleavage site sequence is in italics. Underlined residues in the amino acid sequence are cleaved off by signal peptide peptidases in transport to the periplasm for the native construct or by an in-house TEV-protease during purification for the His-tagged construct.

[b] The gene for OXA-163 was synthesized with optimized codon usage and subcloned into the expression vector.

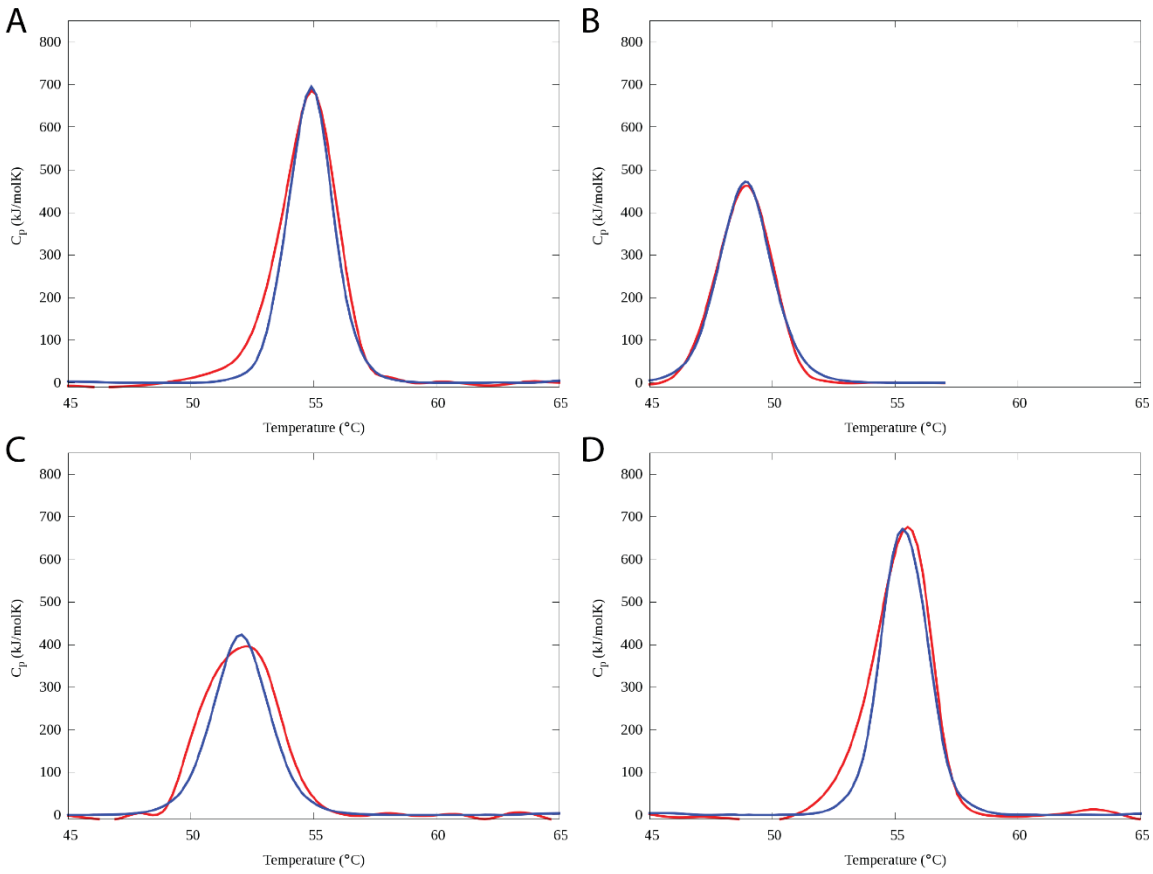

Figure S1 Differential scanning calorimetry curves (red) for (A) OXA-48, (B) OXA-163, (C) OXA-181 and (D) OXA-245 with the theoretical two-state model fitted (blue) for the respective dimers to calculate the ΔH of unfolding.